General Rule to experimental data will evidently depend upon the accuracy of the experimental data. This is a matter for future development and detailed study.

In order to apply the results of this paper to the case of one predominant type of anomalous scatterer, it is only necessary to know the chemical identity of the anomalous scatterer. In the case of more than one type of predominant anomalous scatterer, it is also necessary to have an estimate of the amount of each anomalous scatterer.

I wish to thank Mr Stephen Brenner for writing the appropriate programs and making the computations reported here.

This research was supported in part by USPHS grant GM30902.

References

KARLE J. (1983). *Acta Cryst.* A**39**, 800–805.
KARLE J. (1984*a*). *Acta Cryst.* A**40**, 1–4.
KARLE J. (1984*b*). *Acta Cryst.* A**40**, 4–11.
KARLE J. (1984*c*). *Acta Cryst.* A**40**, 366–373.
PONTENAGEL, W. M. G. F., KRABBENDAM, H., PEERDEMAN, A. F. & KROON, J. (1983). Eighth Eur. Crystallogr. Meet., 8–12 August, Abstract 4.01-P, p. 257.
TIMKOVICH, R. & DICKERSON, R. E. (1976). *J. Biol. Chem.* **251**, 4033–4046.

Acta Cryst. (1984). A**40**, 379–389

Modified Two-Beam Description of X-ray Fields and Intensities near a Three-Beam Diffraction Point. General Formulation and First-Order Solution

BY HELLMUT J. JURETSCHKE

Polytechnic Institute of New York, 333 *Jay Street, Brooklyn, New York* 11201, *USA*

(*Received* 30 *August* 1983; *accepted* 24 *January* 1984)

Abstract

The dynamical three-beam problem in Renninger geometry is cast in a pseudo-two-beam formulation for the primary **0H** reflection, with the inverse of the excitation error ξ_L with respect to the third reciprocal-lattice point **L** acting as a perturbation parameter for modifying the true two-beam solutions. This approach introduces a quasi-universal angular scale x for measuring the onset of all three-beam effects, and it leads to a first-order solution that preserves all features of a two-beam case, but around a shifted Lorentz point, and with modified structure factors. The modified structure factors, odd in x, cause pronounced asymmetries in the diffracted intensities on both sides of the three-beam point, for $|x| \gtrsim 1$. In this range of x, the first-order solution provides a simple *analytic* expression for the integrated diffracted intensity *vs* angle, for a sequence of neighboring three-beam or higher-order points. This is exemplified for the Ge 222 primary reflection. The physics of the onset of the three-beam interaction, and the limitations of the first-order solution are also discussed.

1. Introduction

Multiple diffraction of X-rays in crystals has been fully described mathematically ever since Ewald's (1916) dynamical theory. Its prototype, the two-beam case, has been exhaustively treated analytically (Laue, 1960; James, 1963; Batterman & Cole, 1964), and exploited quantitatively in applications ranging from anomalous transmission (Borrmann, 1950) to interferometry (Bonse & Hart, 1965).

Except in special cases, three-beam or higher interactions have not been describable by equally simple analysis or by general conceptual insights into the nature of the normal modes of propagation. While full computer-implemented solutions of any specific problem exist (*e.g.* Uebach, 1973; Colella, 1974; Kohn, 1979), their conclusions are usually not generalizable, unless statistical sampling of the effects of altering various parameters is undertaken (Hümmer & Billy, 1982).

Recent exploration of the fine structure of multiple interactions ranges from structure-factor phase determination (Post, 1979; Chang, 1982) and surface physics (Cowan, Golovchenko & Robbins, 1980) to nonlinear couplings to other waves (LeRoux, Colella & Bray, 1975; Juretschke & Wasserstein-Robbins, 1982). Hildebrandt (1982) has reviewed other applications. Further work should be stimulated by a description of multiple diffraction that allows a simple mathematical formulation of its basic dynamical features, and relies as much as possible on familiar concepts.

0108-7673/84/040379-11$01.50

In this paper we propose such a description. It concentrates on how the onset of multiple diffraction influences the standard two-beam interaction, such as should occur in the Renninger geometry, by constructing systematic two-beam solutions perturbed by the presence of additional reciprocal-lattice points for diffraction near the Ewald sphere. This approach clearly identifies the increasing importance of different aspects of mutiple diffraction with the strength and order of perturbation. While its solutions cannot describe the center of a given n-point region, they may suffice for many of the currently accessible features of multiple diffraction, given that even for modern collimation this central region is too small to be resolved.

The method differs from most analytic treatments (*e.g.* Hildebrandt, 1967; Ewald & Héno, 1968) by approaching an n-beam point from far away, rather than using it as a starting point. It is most akin to Bethe's (1928) treatment of the influence of weak beams in electron diffraction, where his dynamic potentials are used as a standard perturbation correction. As extended and applied here to X-rays, new features emerge that are characteristic of vector fields, and emphases and interpretations are shifted.

Preliminary accounts of our approach have dealt with the phase problem (Juretschke, 1982*a*, *b*). The systematics of the perturbation method outlined there is worked out below, and then applied to various additional consequences of the first-order theory in perfect crystals. The effects of the next orders of perturbation are the subject of a subsequent report.

Since to first order the effects of more than one additional reciprocal-lattice point are additive, we concentrate on a single three-beam interaction, with **0H** as the primary diffraction, and **L** as the third reciprocal-lattice point. Detailed applications are worked out primarily for the symmetric Bragg case, but the method has general applicability.

2. The central equations and the two-beam limit

This section establishes the general notation and the basic equations, following the treatment of Batterman & Cole (1964), and for further reference summarizes the main results of the two-beam symmetric Bragg case.

In the three-beam case, three X-ray fields interact in a crystal with propagation vectors $\mathbf{K}_0, \mathbf{K}_H, \mathbf{K}_L$ which are related through Bragg's law

$$\mathbf{K}_H = \mathbf{K}_0 + \mathbf{H}, \qquad \mathbf{K}_L = \mathbf{K}_0 + \mathbf{L} \tag{1}$$

via the reciprocal-lattice vectors **0**, **H**, and **L**. All fields have a spatial dependence $\exp(i\mathbf{K}.\mathbf{r})$. In addition to (1), Maxwell's equations require that the associated electric field amplitudes $\mathbf{E}_0, \mathbf{E}_H, \mathbf{E}_L$ must satisfy the three vector equations

$$\begin{aligned} 2k\xi_0\mathbf{E}_0 + k^2\Gamma F_{\bar{H}}\mathbf{E}_H + k^2\Gamma F_{\bar{L}}\mathbf{E}_L &= (\mathbf{K}_0.\mathbf{E}_0)\mathbf{K}_0 \\ k^2\Gamma F_H\mathbf{E}_0 + 2k\xi_H\mathbf{E}_H + k^2\Gamma F_{\bar{L}-\bar{H}}\mathbf{E}_L &= (\mathbf{K}_H.\mathbf{E}_H)\mathbf{K}_H \\ k^2\Gamma F_L\mathbf{E}_0 + k^2\Gamma F_{L-H}\mathbf{E}_H + 2k\xi_L\mathbf{E}_L &= (\mathbf{K}_L.\mathbf{E}_L)\mathbf{K}_L. \end{aligned} \tag{2}$$

Here $k = \omega/c$ is the magnitude of the vacuum propagation vector, $\Gamma = e^2/(\varepsilon_0 m\omega^2 v_{\text{cell}})$ measures the general strength of X-ray scattering, and the individual scattering amplitudes are given by the (complex) structure factors F. The ξ's are the (complex) changes in magnitude of these K vectors from their average within the crystal. Within the approximation implicit in (2) of ignoring all such changes of order higher than Γ, they are given by

$$\xi_i = (\mathbf{K}_i.\mathbf{K}_i)^{1/2} - k(1 - \tfrac{1}{2}\Gamma F_0). \tag{3}$$

In practice, the nine scalar equations of (2) reduce to six equations involving only the three pairs of independent field components transverse to their respective K vectors. Solutions of these six homogeneous equations are characterized by the geometrical condition that the tiepoints of all propagation vector sets (K_0, K_H, K_L) consistent with (1) and (2) lie on a six-sheeted dispersion surface in k space.

Rather than construct this surface in its entirety, we concentrate on its intersections with the two-beam plane of incidence defined by $\mathbf{K}_0$ and $\mathbf{K}_H$. Within this plane we will study the change in form of the dispersion curves as the pure two-beam case is perturbed by the presence of **L**.

Thus the two-beam solution of (1) and (2) serves as a reference. For completeness, we list it below. It is given by two normal modes, σ and π, linearly polarized normal to or within the plane of incidence, with the dispersion relations and field amplitude ratios

$$\begin{aligned} \sigma\text{: } \xi_0\xi_H &= \tfrac{1}{4}k^2\Gamma^2 F_H F_{\bar{H}}, \frac{E_H^\sigma}{E_0^\sigma} = -\frac{k\Gamma F_H}{2\xi_H} \\ \pi\text{: } \xi_0\xi_H &= \tfrac{1}{4}P^2k^2\Gamma^2 F_H F_{\bar{H}}, \frac{E_H^\pi}{E_0^\pi} = -\frac{Pk\Gamma F_H}{2\xi_H}, \end{aligned} \tag{4}$$

where $P = \cos 2\theta_B$, with $\theta_B = \sin^{-1}(H/2k)$ being the geometrical Bragg angle of this interaction.

In absorbing crystals, (4) must be supplemented by boundary conditions that couple the unattenuated exterior ($z > 0$) waves to the lossy interior ($z < 0$) waves, in order to have a complete solution. For a symmetric Bragg reflection, where **H** is normal to the crystal surface ($z = 0$), the boundary conditions impose the relation between ξ_0 and ξ_H:

$$\xi_0 + \xi_H = \delta = k(i\Gamma F_0'' - \Delta\theta \sin 2\theta_B) \tag{5}$$

where $\Delta\theta$ is the deviation of the angles of incidence and reflection from the actual Bragg angle.

As is well known (Afanas'ev & Perstnev, 1969), the integrated intensity of the two-beam reflection in the approximation ignoring absorption in the F_H is given by

$$I=\int \mathrm{d}\theta\left|\frac{E_H}{E_0}\right|^2 = \begin{cases} \dfrac{2\Gamma}{\sin 2\theta_B}\dfrac{|F_H|^2}{|F_H F_{\bar{H}}|^{1/2}}, & \left(\Delta\theta\sim\dfrac{\Gamma F'_H}{\sin 2\theta_B}\right) \\ \dfrac{\pi\Gamma}{4\sin 2\theta_B}\dfrac{|F_H|^2}{F''_0}, & \left(\Delta\theta\sim\dfrac{\Gamma F''_0}{\sin 2\theta_B}\right), \end{cases} \tag{6}$$

depending on whether $|F'_H|\gg|F''_0|$ (strong reflection) or $|F'_H|\ll|F''_0|$ (weak reflection), in the two limits. The brackets on the right side give the angular ranges for the main contribution to each integral.

3. Geometrical relations – the symmetric Bragg case

The reduction of (2) to six scalar transverse equations will be carried out using the orthogonal coordinate system (k_x, k_y, k_z) shown in Fig. 1. The k_x-k_z plane is the two-beam plane of incidence, and the origin of coordinates is at the Lorentz point in this plane. In the conventional linear approximation the geometrical three-beam Lorentz point lies somewhere along the k_y axis, and is here given the coordinates $(0, -k\cos\theta_B\tan\varphi_T, 0)$.

For a tiepoint $(k_x, 0, k_z)$ in the plane of incidence, the three K vectors have the components

$$\begin{aligned} \mathbf{K}_0 &= (k'\cos\theta_B - k_x, 0, -k'\sin\theta_B - k_z - i\kappa) \\ \mathbf{K}_H &= (k'\cos\theta_B - k_x, 0, k'\sin\theta_B - k_z - i\kappa) \\ \mathbf{K}_L &= (k'\cos\theta_L\cos\varphi_L - k_x, k'\cos\theta_L\sin\varphi_L \\ &\quad - k\cos\theta_B\tan\varphi_T, k'\sin\theta_L - k_z - i\kappa), \end{aligned} \tag{7}$$

where $k'=k(1-\frac{1}{2}\Gamma F'_0)$ is the magnitude of the real part of the average propagation vector inside the crystal.

The angles θ_L and φ_L (Fig. 1) define the direction of $\mathbf{K}_L$. Only the z components in (7) contain an imaginary part, since because of (1) all K vectors can at most have a common imaginary component normal to the crystal surface.

Substitution of (7) in the right side of (3) connects the set ξ_0, ξ_H, ξ_L to k_x, k_y, k_z:

$$\begin{aligned} \xi_0 &= -k_x\cos\theta_B + (k_z+i\kappa)\sin\theta_B + \tfrac{1}{2}ik\Gamma F''_0 \\ \xi_H &= -k_x\cos\theta_B - (k_z+i\kappa)\sin\theta_B + \tfrac{1}{2}ik\Gamma F''_0 \\ \xi_L &= -k_x\cos\theta_L\cos\varphi_L - k\cos\theta_B\tan\varphi_T\cos\theta_L\sin\varphi_L \\ &\quad -(k_z+i\kappa)\sin\theta_L + \tfrac{1}{2}ik\Gamma F''_0. \end{aligned} \tag{8}$$

Since $k_x = k\Delta\theta\sin\theta_B$ is fixed by the incident-beam angle $\Delta\theta$ relative to the actual Bragg angle, the sum of the first two equations in (8) reduces to (5). The third equation in (8) relates ξ_L to the other ξ's:

$$\xi_L = -k\cos\theta_B\tan\varphi_T\cos\theta_L\sin\varphi_L + \frac{\cos\theta_L\cos\varphi_L}{2\cos\theta_B}\delta' - \frac{\sin\theta_L}{2\sin\theta_B}(2\xi_0-\delta) + \tfrac{1}{2}ik\Gamma F''_0. \tag{9}$$

Hence, using (5) and (9), we can express all ξ's in (2) in terms of one, *e.g.* ξ_0.

In what follows, we make particular use of the fact that in the active two-beam region δ and ξ_0 are small, while $k\tan\varphi_T$ can be much larger, so that for a wide range of φ_T (9) can be approximated by its first term. For the time being, however, we will retain the entire form of (9).

The transverse electric-field amplitudes can be separated into orthogonal σ and π components in the real-space coordinate system x, y, z analogous to that of Fig. 1, by following the prescription defined in § 2:

$$\begin{aligned} \mathbf{E}_0^\sigma &= E_0^\sigma(0,1,0) \\ \mathbf{E}_H^\sigma &= E_H^\sigma(0,1,0) \\ \mathbf{E}_L^\sigma &= E_L^\sigma(-\sin\varphi_L, \cos\phi_L, 0) \end{aligned} \tag{10}$$

and

$$\begin{aligned} \mathbf{E}_0^\pi &= E_0^\pi(\sin\theta_B, 0, \cos\theta_B) \\ \mathbf{E}_H^\pi &= E_H^\pi(-\sin\theta_B, 0, \cos\theta_B) \\ \mathbf{E}_L^\pi &= E_L^\pi(-\sin\theta_L\cos\varphi_L, -\sin\theta_L\sin\varphi_L, \cos\theta_L). \end{aligned} \tag{11}$$

The 0 and H fields follow the conventional definitions of σ and π polarizations. The directions of $\mathbf{E}_L^\sigma$ and $\mathbf{E}_L^\pi$ are chosen to have $\mathbf{E}_L^\sigma$ lie in the k_x–k_y plane, and with $\mathbf{E}_L^\pi$ along $\mathbf{K}_L\times\mathbf{E}_L^\sigma$, so that for $\varphi_L=0$ these fields also reduce to the conventional two-beam polarizations.

With the definitions (7), (10) and (11), we can construct all the transverse fields contained in (2). For example, the first equation in (2) must involve the projections of all fields on the directions of either

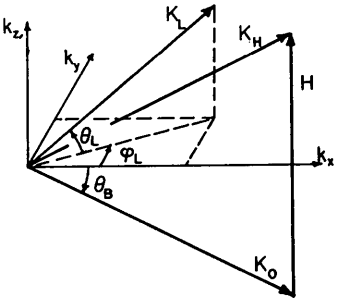

Fig. 1. Local coordinate system in k space, with the two-beam Lorentz point at the origin in the **0H** plane of incidence. θ_L and φ_L define the direction of $\mathbf{K}_L$. As shown, the tie point of the **K**'s and the geometrical three-beam Lorentz point are also at the origin, but both may be elsewhere.

$\mathbf{E}_0^\sigma$ or $\mathbf{E}_0^\pi$. These are, for $\mathbf{E}_0$, $\mathbf{E}_H$, and $\mathbf{E}_L$, respectively,

along $\mathbf{E}_0^\sigma$: E_0^σ, E_H^σ, $E_L^\sigma \cos\varphi_L - E_L^\pi \sin\theta_L \sin\varphi_L$;

along $\mathbf{E}_0^\pi$: E_0^π, $E_H^\pi \cos 2\theta_B$,

$-E_L^\sigma \sin\theta_B \sin\varphi_L$

$+E_L^\pi(-\sin\theta_B \sin\theta_L \cos\varphi_L + \cos\theta_B \cos\theta_L)$.

4. General pseudo-two-beam formulation

The projection approach outlined in the last two sections leads to the six transverse equations contained in (2). According to their σ or π character, they can be grouped in two sets:

$$\begin{aligned}
&2\xi_0 E_0^\sigma + k\Gamma F_{\bar{H}} E_H^\sigma + k\Gamma F_{\bar{L}}(P_x E_L^\sigma - P_{xz} E_L^\pi) = 0\\
&k\Gamma F_H E_0^\sigma + 2\xi_H E_H^\sigma + k\Gamma F_{\bar{L}-\bar{H}}(P_x E_L^\sigma - P_{xz} E_L^\pi) = 0\\
&k\Gamma F_L(P_x E_0^\sigma - P_{0x} E_0^\pi) + k\Gamma F_{L-H}(P_x E_H^\sigma + P_{0x} E_H^\pi)\\
&\quad + 2\xi_L E_L^\sigma = 0
\end{aligned} \tag{12a}$$

and

$$\begin{aligned}
&2\xi_0 E_0^\pi + k\Gamma P F_{\bar{H}} E_H^\pi\\
&\quad + k\Gamma F_{\bar{L}}[-P_{0x} E_L^\sigma + (P_{0z} - P_{0xz}) E_L^\pi] = 0\\
&k\Gamma P F_H E_0^\pi + 2\xi_H E_H^\pi\\
&\quad + k\Gamma F_{\bar{L}-\bar{H}}[P_{0x} E_L^\sigma + (P_{0z} + P_{0xz}) E_L^\pi] = 0\\
&k\Gamma F_L[-P_{xz} E_0^\sigma + (P_{0z} - P_{0xz}) E_0^\pi]\\
&\quad + k\Gamma F_{L-H}(-P_{xz} E_H^\sigma + (P_{0z} + P_{0xz}) E_H^\pi) + 2\xi_L E_L^\pi = 0.
\end{aligned} \tag{12b}$$

The P's are combinations of the geometrical factors appearing in (10) and (11), given by

$$\begin{aligned}
P = \cos 2\theta_B,\ P_x = \cos\varphi_L,\ P_{0x} = \sin\theta_B \sin\varphi_L,\\
P_{0z} = \cos\theta_B \cos\theta_L,\ P_{xz} = \sin\varphi_L \sin\theta_L,\\
P_{0xz} = \sin\theta_B \cos\varphi_L \sin\theta_L.
\end{aligned} \tag{13}$$

Since our main interest is in the fields propagating along $\mathbf{K}_0$ and $\mathbf{K}_H$, we now eliminate E_L^σ and E_L^π from (12). This procedure introduces the factor $1/\xi_L$ in all terms resulting from the L fields, and thus identifies this quantity as a convenient perturbation expansion parameter.

By solving the last lines of (12a) and (12b) for E_L^σ and E_L^π, and substituting for these fields in the four other lines, we obtain the following four equations, again written in two groups:

$$\begin{aligned}
&\left(2\xi_0 - \frac{k^2\Gamma^2 F_L F_{\bar{L}}}{2\xi_L}\Pi_1\right) E_0^\sigma\\
&\quad + k\Gamma\left(F_{\bar{H}} - \frac{k\Gamma F_{\bar{L}} F_{L-H}}{2\xi_L}\Pi_1\right) E_H^\sigma\\
&\quad + \frac{k^2\Gamma^2 F_{\bar{L}}}{2\xi_L}(F_L \Pi_2 E_0^\pi - F_{L-H}\Pi_3 E_H^\pi) = 0
\end{aligned} \tag{14a}$$

$$\begin{aligned}
&k\Gamma\left(F_H - \frac{k\Gamma F_L F_{\bar{L}-\bar{H}}}{2\xi_L}\Pi_1\right) E_0^\sigma\\
&\quad + \left(2\xi_H - \frac{k^2\Gamma^2 F_{L-H} F_{\bar{L}-\bar{H}}}{2\xi_L}\Pi_1\right) E_H^\sigma\\
&\quad + \frac{k^2\Gamma^2 F_{\bar{L}-\bar{H}}}{2\xi_L}(F_L \Pi_2 E_0^\pi - F_{L-H}\Pi_3 E_H^\pi) = 0
\end{aligned}$$

and

$$\begin{aligned}
&\left(2\xi_0 - \frac{k^2\Gamma^2 F_L F_{\bar{L}}}{2\xi_L}\Pi_4\right) E_0^\pi\\
&\quad + k\Gamma\left(P F_{\bar{H}} - \frac{k\Gamma F_{\bar{L}} F_{L-H}}{2\xi_L}\Pi_6\right) E_H^\pi\\
&\quad + \frac{k^2\Gamma^2 F_{\bar{L}}}{2\xi_L}\Pi_2(F_L E_0^\sigma + F_{L-H} E_H^\sigma) = 0\\
&k\Gamma\left(P F_H - \frac{k\Gamma F_L F_{\bar{L}-\bar{H}}}{2\xi_L}\Pi_6\right) E_0^\pi\\
&\quad + \left(2\xi_H - \frac{k^2\Gamma^2 F_{L-H} F_{\bar{L}-\bar{H}}}{2\xi_L}\Pi_5\right) E_H^\pi\\
&\quad - \frac{k^2\Gamma^2 F_{\bar{L}-\bar{H}}}{2\xi_L}\Pi_3(F_L E_0^\sigma + F_{L-H} E_H^\sigma) = 0.
\end{aligned} \tag{14b}$$

The factors Π_1 to Π_6 appearing in (14) are new combinations of the geometrical terms defined in (13):

$$\begin{aligned}
\Pi_1 &= P_x^2 + P_{xz}^2\\
\Pi_2 &= P_x P_{0x} + (P_{0z} - P_{0xz}) P_{xz}\\
\Pi_3 &= P_x P_{0x} - (P_{0z} + P_{0xz}) P_{xz}\\
\Pi_4 &= P_{0x}^2 + (P_{0z} - P_{0xz})^2\\
\Pi_5 &= P_{0x}^2 + (P_{0z} + P_{0xz})^2\\
\Pi_6 &= -P_{0x}^2 + P_{0z}^2 - P_{0xz}^2.
\end{aligned} \tag{15}$$

Equations (14) can be simplified formally by introducing reduced variables. Let us refer all ξ's to the common scale $k\Gamma$, and to appropriately shifted origins:

$$\begin{aligned}
\tilde{\xi}_L &= \xi_L / k\Gamma,\\
\tilde{\xi}_0^\sigma &= \xi_0 / k\Gamma - \frac{1}{4}\frac{F_L F_{\bar{L}}}{\tilde{\xi}_L}\Pi_1,\\
\tilde{\xi}_0^\pi &= \xi_0 / k\Gamma - \frac{1}{4}\frac{F_L F_{\bar{L}}}{\tilde{\xi}_L}\Pi_4,\\
\tilde{\xi}_H^\sigma &= \xi_H / k\Gamma - \frac{1}{4}\frac{F_{L-H} F_{\bar{L}-\bar{H}}}{\tilde{\xi}_L}\Pi_1,\\
\tilde{\xi}_H^\pi &= \xi_H / k\Gamma - \frac{1}{4}\frac{F_{L-H} F_{\bar{L}-\bar{H}}}{\tilde{\xi}_L}\Pi_5.
\end{aligned} \tag{16a}$$

In addition, we introduce the modified structure factors

$$F^{\sigma}_{HL} = F_H - F_{\bar{L}}F_{L-H}/2\tilde{\xi}_L\Pi_1,$$
$$F^{\pi}_{HL} = PF_H - \frac{F_{\bar{L}}F_{L-H}}{2\tilde{\xi}_L}\Pi_6. \tag{16b}$$

Using (16), the four lines of (14) take the compact form

$$\begin{aligned}
&2\tilde{\xi}^{\sigma}_0 E^{\sigma}_0 + F^{\sigma}_{H\bar{L}}E^{\sigma}_H + \frac{1}{2}\frac{F_{\bar{L}}F_L}{\tilde{\xi}_L}\Pi_2 E^{\pi}_0 \\
&\quad -\frac{1}{2}\frac{F_{\bar{L}}F_{L-H}}{\tilde{\xi}_L}\Pi_3 E^{\pi}_H = 0 \\
&F^{\sigma}_{HL}E^{\sigma}_0 + 2\tilde{\xi}^{\sigma}_H E^{\sigma}_H + \frac{1}{2}\frac{F_{\bar{L}-\bar{H}}F_L}{\tilde{\xi}_L}\Pi_2 E^{\pi}_0 \\
&\quad -\frac{1}{2}\frac{F_{\bar{L}-\bar{H}}F_{L-H}}{\tilde{\xi}_L}\Pi_3 E^{\pi}_H = 0 \\
&\frac{1}{2}\frac{F_{\bar{L}}F_L}{\tilde{\xi}_L}\Pi_2 E^{\sigma}_0 + \frac{1}{2}\frac{F_{\bar{L}}F_{L-H}}{\tilde{\xi}_L}\Pi_2 E^{\sigma}_H \\
&\quad +2\tilde{\xi}^{\pi}_0 E^{\pi}_0 + F^{\pi}_{H\bar{L}}E^{\pi}_H = 0 \\
&\quad -\frac{1}{2}\frac{F_{\bar{L}-\bar{H}}F_L}{\tilde{\xi}_L}\Pi_3 E^{\sigma}_0 - \frac{1}{2}\frac{F_{\bar{L}-\bar{H}}F_{L-H}}{\tilde{\xi}_L}\Pi_3 E^{\sigma}_H \\
&\quad +F^{\pi}_{HL}E^{\pi}_0 + 2\tilde{\xi}^{\pi}_H E^{\pi}_H = 0.
\end{aligned} \tag{17}$$

The secular equation following from (17), that defines the dispersion surface, can be put into the form

$$\begin{aligned}
&(\tilde{\xi}^{\sigma}_0\tilde{\xi}^{\sigma}_H - \tfrac{1}{4}F^{\sigma}_{HL}F^{\sigma}_{H\bar{L}})(\tilde{\xi}^{\pi}_0\tilde{\xi}^{\pi}_H - \tfrac{1}{4}F^{\pi}_{HL}F^{\pi}_{H\bar{L}}) \\
&= \frac{1}{16\tilde{\xi}^2_L}[F_{L-H}F_{\bar{L}-\bar{H}}\tilde{\xi}^{\sigma}_0 + F_L F_{\bar{L}}\tilde{\xi}^{\sigma}_H \\
&\quad -\tfrac{1}{2}(F_{\bar{L}}F_{L-H}F^{\sigma}_{HL} + F_L F_{\bar{L}-\bar{H}}F^{\sigma}_{H\bar{L}})] \\
&\quad \times[F_{L-H}F_{\bar{L}-\bar{H}}\Pi^2_3\tilde{\xi}^{\pi}_0 + F_L F_{\bar{L}}\Pi^2_2\tilde{\xi}^{\pi}_H \\
&\quad +\tfrac{1}{2}\Pi_2\Pi_3(F_{\bar{L}}F_{L-H}F^{\pi}_{HL} + F_L F_{\bar{L}-\bar{H}}F^{\pi}_{H\bar{L}})].
\end{aligned} \tag{18}$$

Together, (17) and (18) represent an exact formulation of the three-beam problem, cast in terms of modified variables. Note that because of (16*a*) the pairs of variables $\tilde{\xi}^{\sigma}_0$, $\tilde{\xi}^{\pi}_0$ and $\tilde{\xi}^{\sigma}_H$, $\tilde{\xi}^{\pi}_H$ are not independent. The exact two-beam case occurs in the limit $1/\tilde{\xi}_L \to 0$. For finite $1/\tilde{\xi}_L$, a non-vanishing right side of (18) implies that the normal modes of propagation in the crystal are no longer plane polarized. Equation (18) also brings out the differences in the perturbation approach for X-rays and electrons. For the latter, it becomes (Gjønnes, 1962):

$$(\tilde{\xi}_0\tilde{\xi}_H - \tfrac{1}{4}F_{HL}F_{H\bar{L}}) = 0,$$

which corresponds to the first bracket of (18) alone, with $\Pi_1 = 1$, in consonance with the fact that electron fields are scalar.

Since the geometrical decomposition of the fields of § 3 relies entirely on a coordinate system tied to **H** and is independent of any boundary conditions, (17) and (18) are valid for all three-beam cases. Other directions of the crystal surface relative to **H** only modify (7) to (9). Thus, for the symmetric Laue case the relations between the ξ's become:

$$\begin{aligned}
&\xi_0 - \xi_H = -\delta = k\sin 2\theta_B\,\Delta\theta \\
&\xi_L = -k\cos\theta_B\tan\varphi_T\cos\theta_L\sin\varphi_L + \frac{\sin\theta_L}{2\sin\theta_B}\delta \\
&\quad + \frac{\cos\theta_L\cos\varphi_L}{2\cos\theta_B}(2\xi_0 + \delta) \\
&\quad + \frac{i}{2}\left(1 - \frac{\cos\theta_L\cos\varphi_L}{\cos\theta_B}\right)(k\Gamma F''_0)
\end{aligned} \tag{19}$$

so that here δ is purely real. Since the leading term in ξ_L is the same as in (9), all conclusions based on it alone in the Bragg case also remain valid in the Laue case.

5. The first-order solution and its range of validity

The underlying criterion for treating the three-beam case as a pseudo-two-beam case is that ξ_L can be taken as parameter rather than as a dynamical variable, or that ξ_L can be approximated by the first term in (9). Since we are interested in solutions close to the two-beam region of total reflection where ξ_0, ξ_H and δ are all of the same order of magnitude as $k\Gamma F_H$ (or $k\Gamma F''_0$), or less, this approximation should be valid as long as

$$\tan\varphi_T \gg \Gamma F_H, \Gamma F''_0 \tag{20}$$

or, from (6), when φ_T is much larger than the width of the primary reflection. This is not a very strong restriction.

Within this pseudo-two-beam framework, an exact analytic solution of (18), a fourth-order equation in, say, $\tilde{\xi}^{\sigma}_0$, is still not generally obtainable. But approximate analytic solutions are possible, as perturbations on the pure two-beam solution. *We define the first-order solution as that obtained when the right side of* (18) *is set equal to zero.*

This solution is evidently correct to power $1/\tilde{\xi}_L$ in all variables. It also includes those corrections to second order that still allow the left side to be obviously factorable, and therefore in a form closely resembling that of an exact two-beam case.

It is difficult to establish a precise criterion for the validity of this truncated solution, because of the various geometrical factors and the occurrence of the variables $\tilde{\xi}$ on the right side of (18). Since typical terms on that side are small compared to typical terms on the other side when

$$\tilde{\xi}_L \gg \frac{1}{2}\frac{|F_L||F_{L-H}|}{|F_H|} \tag{21}$$

this inequality should serve as a rough, and probably conservative, measure.

For three strong F's, with reflection widths typically of a few seconds of arc, (20) and (21) are equivalent, so the first-order solution should be good for φ_T as small as a minute, or less. For a weak primary reflection F_H, with the other two strong, (21) predominates, and the first-order solution may break down at larger angles. Since many of the interesting features of the onset of three-beam effects scale in angle as (21), these continue to be describable by first-order theory.

As already mentioned, the proposed first-order solution goes beyond first order in $1/\xi_L$ by including terms to 'complete the square' in each left side bracket of (18). This inclusion defines the most general solutions retaining the σ and π normal modes of the two-beam case. More exact higher-order solutions must treat the mode coupling, including the case that the starting modes are degenerate.

6. General features of the first-order solution

When the right side of (18) is set equal to zero, the solutions of the three-beam problem correspond to the traditional σ- and π-polarized normal modes of the underlying two-beam case. The only changes are that the structure factors are modified, and that the Lorentz points are shifted. All other physical consequences are exactly those of the two-beam case summarized in § 2.

Further discussion is simplified by introducing a scale parameter for φ_T that is naturally adjusted to the limit of validity established by (21). Let

$$\frac{1}{x}=-\frac{F_L F_{\bar{L}-\bar{H}}}{F_H}\frac{\Pi_1}{2\tilde{\xi}_L}$$
$$\left[=\frac{\Gamma}{2\tan\varphi_T}\left(\frac{F_L F_{\bar{L}-\bar{H}}}{F_H}\frac{\Pi_1}{\cos\theta_B\cos\theta_L\sin\varphi_L}\right)\right]. \quad (22)$$

Then (16b) becomes

$$F^{\sigma}_{HL}=F_H\left(1+\frac{1}{x}\right),\qquad F^{\pi}_{HL}=F_H\left(P+\frac{\Pi_6}{\Pi_1}\frac{1}{x}\right) \quad (23)$$

and the integrated intensities following from (6) relative to that of the exact σ two-beam case are

$$\frac{I^{\sigma}_{HL}}{I^{\sigma}_{H}}=\left|1+\frac{1}{x}\right|^n,\qquad \frac{I^{\pi}_{HL}}{I^{\sigma}_{H}}=\left|P+\frac{\Pi_6}{\Pi_1}\frac{1}{x}\right|^n, \quad (24)$$

where the exponent n varies from 1 to 2 as the primary reflection changes from strong to weak.

The most dramatic consequence of (24) is that it predicts a universal description of the effect of **L** on the relative **0H** integrated intensity in terms of the angular scale based on (the real part of) x. Furthermore, (24) is strongly asymmetric with respect to the sign reversal of x, producing intensity enhancements and reductions on opposite sides of the three-beam point $\varphi_T=0$, with the sign of x relative to that of φ_T fixed by the (invariant) phase of the combination $(F_L F_{\bar{L}-\bar{H}}/F_H)$. The application of this behavior to phase determinations in centrosymmetric and noncentrosymmetric structures has already been discussed (Juretschke, 1982*a*, *b*), and attention has been drawn to the possibility that the sign of Π_6/Π_1 may introduce an additional reversal of asymmetry between the σ and π modes.

If x is largely real, (24) in fact predicts a vanishing reflected **0H** intensity at $x=-1$, or $x=-\Pi_6/P\Pi_1$, for the two polarizations. How strongly this prediction is actually fulfilled depends sensitively on the exact range of validity of the first-order solution. For x of order unity, both sides of (21) are of similar magnitude, and unless (21) sets a conservative criterion in any specific case, the minimum of intensity will probably be less pronounced. This, however, in no way affects the asymmetries in (24) predicted for larger x. A closely related vanishing of structure factors has been seen in electron diffraction (Watanabe, Uyeda & Kogiso, 1968).

Because of the shifts of origin introduced in (16a), the first-order solution also contains a shift in the two-beam Lorentz point as a function of x. For σ polarization it is

$$\Delta k_x=\frac{k\Gamma F_H}{4\cos\theta_B}\left[\left(\frac{F_{\bar{L}}}{F_{\bar{L}-\bar{H}}}+\frac{F_{L-H}}{F_L}\right)\frac{1}{x}\right]'$$
$$\Delta k_z=-\frac{k\Gamma F_H}{4\sin\theta_B}\left[\left(\frac{F_{\bar{L}}}{F_{\bar{L}-\bar{H}}}-\frac{F_{L-H}}{F_L}\right)\frac{1}{x}\right]', \quad (25)$$

where the prime indicates the real part. For π polarization, the same expressions hold if the first term in each inner bracket is multiplied by Π_4/Π_1, and the second by Π_5/Π_1. This shift is also antisymmetric in x, but, being proportional to Γ^2, will generally be very small, of the order of a fraction of a second, for $|x|\gtrsim 1$. It implies that the approach to the three-beam Lorentz point is not monotonic. The imaginary parts of the shifts in (16a) will modify the absorption.

The first-order solution also predicts scattering into the K_L channel. From (12a) and (12b), the relative field amplitudes for each mode are:

$$\frac{E^{\sigma}_L}{E^{\sigma}_0}=\frac{1}{x}\frac{F_H}{F_{\bar{L}-\bar{H}}}\frac{P_x}{\Pi_1}\left(1+\frac{F_{L-H}}{F_L}\frac{E^{\sigma}_H}{E^{\sigma}_0}\right)$$
$$\frac{E^{\pi}_L}{E^{\sigma}_0}=-\frac{1}{x}\frac{F_H}{F_{\bar{L}-\bar{H}}}\frac{P_{xz}}{\Pi_1}\left(1+\frac{F_{L-H}}{F_L}\frac{E^{\sigma}_H}{E^{\sigma}_0}\right) \quad (26a)$$
$$\frac{E^{\sigma}_L}{E^{\pi}_0}=-\frac{1}{x}\frac{F_H}{F_{\bar{L}-\bar{H}}}\frac{P_{0x}}{\Pi_1}\left(1-\frac{F_{L-H}}{F_L}\frac{E^{\pi}_H}{E^{\pi}_0}\right)$$
$$\frac{E^{\pi}_L}{E^{\pi}_0}=\frac{1}{x}\frac{F_H}{F_{\bar{L}-\bar{H}}}\frac{1}{\Pi_1}\left[P_{0z}-P_{0xz}+\frac{F_{L-H}}{F_L}(P_{0z}+P_{0xz})\frac{E^{\pi}_H}{E^{\pi}_0}\right]. \quad (26b)$$

As expected, the intensity along $\mathbf{K}_L$ varies like $1/x^2$. As $|x|$ approaches unity, (26) predicts comparable intensities for the **0H** and **0L** reflections. Note, however, that in this range of x the **0L** intensities are explicitly symmetric in x, and any asymmetry as a function of φ_T must lie inside the brackets in (26). For weak primary reflections, these brackets are always of order unity. In that case the relative integrated intensities in the $\mathbf{K}_L$ direction corresponding to (24) are

$$\frac{I_L(\sigma)}{I_H^\sigma}=\frac{1}{|x|^2}\frac{1}{\Pi_1}\frac{|F_0''|^2}{|F_{\bar{L}-\bar{H}}|^2},$$
$$\frac{I_L(\pi)}{I_H^\sigma}=\frac{1}{|x|^2}\frac{|\Pi_4|}{\Pi_1^2}\frac{|F_0''|^2}{|F_{L-\bar{H}}|^2}. \qquad (27)$$

For strong reflections, there may either be some enhancement or a diminution, depending on the net sign and the magnitude of the term modifying unity in each bracket.

One limitation of this solution must be noted. The angular factor in the denominator of (22) is proportional to the projection of $\mathbf{K}_L$ on the k_y axis. As this projection decreases, the condition $|x|\sim 1$ occurs at increasingly larger φ_T, so that the features described above also do. For $\mathbf{K}_L$ in the plane of incidence, the three-beam Lorentz point is always in the k_x-k_z plane. The first term in (9) vanishes, and ξ_L is always a dynamical variable.

7. The Ge 222/11$\bar{1}$ interaction

Equations (24) and (25) summarize the most important formal results of the first-order solution. We will apply them to the specific case of Ge, $H=222$ and $L=11\bar{1}$, which has already received considerable experimental and computational attention. Table 1 lists the parameters applying here, and Fig. 2 shows the result of using (24) with $n=2$. The scale connecting x and φ_T is, using the data of Table 1 in (22), $\tan\varphi_T=2{\cdot}21\times10^{-3}\,x$, or $|\varphi_T|=7{\cdot}60$ minutes of arc when $|x|=1$. The figure includes both σ and π intensities, and the inset shows the details of the intensity variation for both polarizations around the minima near $x=-1$. For all $|x|\geq 1$, the predominant σ contribution of Fig. 2 should be compared to experiment, usually carried out with unpolarized incident radiation. As shown in the next section, the comparison with recent high-resolution experiments (Nicolosi, 1982) is very satisfactory, in the overall asymmetry of the intensity as well as in the location of the minimum, even without making allowance for any of the usual experimental divergences. Comparison with an exact computer solution of this case (Chang, 1982) is equally satisfactory. Thus, at least for integrated properties, the simple analytic form of (24) contains the major elements of this three-beam interaction in the interesting region $|x|\geq 1$.

Table 1. *Numerical inputs for the Ge 222/11$\bar{1}$ interaction*

Cu $K\alpha$ radiation	$k(=2\pi/\lambda)=4{\cdot}08\times10^8$ cm^{-1}	
Ge 222 reflection	$\theta_B=28{\cdot}15°$,	$\Gamma=1{\cdot}175\times10^{-7}$
	$F_{222}=1{\cdot}0$,	$F''_{000}=7{\cdot}35$
Coupling parameters to $11\bar{1}$	$F_{11\bar{1}}=151$,	$\varphi_L=-27{\cdot}80°$
	$F_{\bar{1}\bar{1}\bar{3}}=-121$,	$\theta_L=-18{\cdot}33°$
Angular parameters of (13) and (15)	$P=0{\cdot}5549$,	$P_x=0{\cdot}8846$
	$P_{0x}=-0{\cdot}2200$,	$P_{0z}=0{\cdot}8370$
	$P_{xz}=0{\cdot}1467$,	$P_{0xz}=-0{\cdot}1312$
	$\Pi_1=0{\cdot}8040$,	$\Pi_2=-0{\cdot}0526$
	$\Pi_3=-0{\cdot}2982$,	$\Pi_4=0{\cdot}9858$
	$\Pi_5=0{\cdot}5466$,	$\Pi_6=0{\cdot}6350$

From (27), the relative integrated intensities going into the $\mathbf{K}_L$ direction are proportional to $|F_0''|^2/|F_{\bar{L}-\bar{H}}|^2=0{\cdot}0037$, so that even for $|x|=1$ they are negligible compared to the variations of the **0H** intensity.

As a test of the goodness of the first-order solution, we have evaluated the right side of (18), using the left-side solutions that assume it to be zero, in two ways. In the first, the right side residual, designated by $S(\delta, x)$, is determined starting from either of the first-order σ or π solutions (ξ_0, ξ_H) for a given δ of the left, and then applying the relations (16*a*) to interconnect with the remaining ξ's appearing in S. In the second way, both σ and π first-order solutions are used simultaneously to evaluate S. The results of these procedures are shown in Tables 2(*a*) and 2(*b*), which list the absolute values $|S^\sigma|$ and $|S^\pi|$ obtained by the first approach, and the value $|S|$ obtained by the second, all in the range of $\tilde{\delta}'$ which contributes most to the integrated intensity. The common scale for all variables is that introduced in (16*a*).

All values of S lie below unity. This occurs in a region where the complex $\tilde{\delta}$ is always of order 10 and

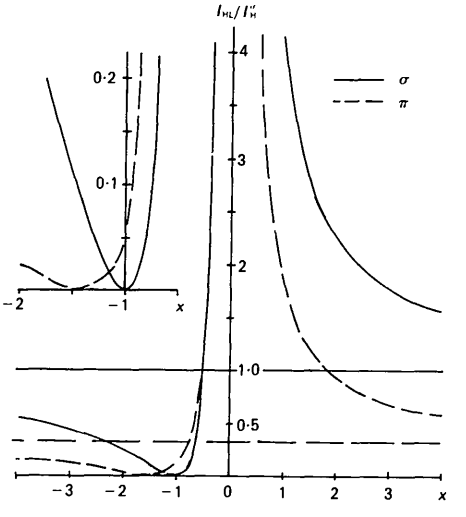

Fig. 2. Ge 222/11$\bar{1}$. Integrated **0H** intensities I_{HL} *vs* x relative to the two-beam primary reflection I_H^σ, according to (24). The inset enlarges the region near $x=-1$.

Table 2. *Absolute values of the residual of the right side of* (18) *for* Ge 222/11$\bar{1}$

Each triplet lists $|S^{\sigma}|$, $|S^{\pi}|$, and $|S|$, evaluated as explained in the text, below each other.

	$\tilde{\delta}'=$ 10	5	2	0	−2	−5	−10
(*a*) $x<0$							
x							
	0·076	0·036	0·026	0·022	0·022	0·029	0·056
−2·0	0·067	0·035	0·025	0·023	0·024	0·031	0·061
	0·105	0·054	0·039	0·035	0·037	0·049	0·095
	0·141	0·073	0·050	0·042	0·040	0·048	0·091
−1.5	0·126	0·065	0·046	0·040	0·041	0·053	0·103
	0·196	0·101	0·071	0·063	0·064	0·083	0·161
	0·215	0·113	0·077	0·064	0·059	0·067	0·123
−1·25	0·189	0·098	0·068	0·059	0·058	0·074	0·142
	0·294	0·151	0·106	0·091	0·091	0·115	0·222
	0·366	0·195	0·133	0·109	0·097	0·102	0·173
−1·0	0·315	0·163	0·112	0·094	0·090	0·109	0·207
	0·488	0·252	0·173	0·147	0·141	0·171	0·324
	0·744	0·407	0·281	0·228	0·198	0·189	0·266
−0·75	0·618	0·324	0·219	0·179	0·162	0·180	0·329
	0·956	0·501	0·339	0·278	0·252	0·282	0·516
(*b*) $x>0$							
x							
	0·221	0·204	0·251	0·299	0·365	0·508	0·884
0·75	0·262	0·182	0·200	0·234	0·287	0·409	0·741
	0·410	0·285	0·314	0·367	0·447	0·634	1·145
	0·137	0·101	0·117	0·140	0·173	0·246	0·441
1·0	0·163	0·102	0·103	0·118	0·144	0·207	0·381
	0·256	0·159	0·162	0·185	0·225	0·321	0·591
	0·096	0·062	0·068	0·080	0·100	0·143	0·261
1·25	0·112	0·066	0·063	0·071	0·086	0·124	0·231
	0·175	0·103	0·099	0·111	0·134	0·193	0·358
	0·071	0·043	0·044	0·052	0·064	0·093	0·172
1·5	0·081	0·046	0·043	0·048	0·057	0·082	0·155
	0·127	0·072	0·068	0·074	0·089	0·128	0·240
	0·044	0·024	0·023	0·027	0·033	0·048	0·090
2·0	0·048	0·027	0·024	0·026	0·031	0·044	0·083
	0·075	0·042	0·037	0·040	0·048	0·068	0·129

implies an appreciable internal cancellation of terms in S, and confirms the goodness of the first-order solutions. All $|S|$ values decrease towards the Lorentz point corresponding to each x, and since the actual complex function S swings through roughly 180° in passing through this region, its effects on any integrated properties are further minimized. As expected, all $|S|$ values increase as $|x|$ decreases, and the numbers in Tables 2 suggest that for $|x|<1$ the right side of (18) cannot be neglected. This agrees with the estimates of § 5, now applied to a weak primary reflection.

To get an idea of how well the criteria involving S apply to a strong primary reflection, we have examined the same 222/11$\bar{1}$ case, but now arbitrarily setting $F_0''=0$. Fig. 3 shows $|S|$ obtained for the same range of negative x as in Table 2(*a*), plotted against $\tilde{k}_x=k_x/(\Gamma k)$. From (5) and (6), the strong reflection occurs in the range $\tilde{k}_x=\pm|F_{HL}|/2\cos\theta_B=\pm|1+1/x|/1{\cdot}763$, relative to the shifted Lorentz point of (25). Over this range S is exceedingly small, except for $|x|<1$. The $|S|$ in Fig. 3 are much smaller than those of Table 2 because here the real part of $\tilde{\delta}$ sets the measure of smallness in (18), while in Table 2 it is controlled by the large constant imaginary part of $\tilde{\delta}$.

Hence, the first-order solution gives a good approximation for $|x|\gtrsim 1$, for both weak and strong primary reflections, at least for the chosen combination of F's and **H, L**.

The hypothetical strong reflection case is used in § 9 to explore some of the underlying physics of the first-order solution.

8. Applications of the first-order solution

The basic first-order solution of a three-beam interaction of § 6 can be easily extended to other multiple-beam interactions. This section discusses some of these extensions under separate subheadings.

A. Many neighboring three-beam cases

As the angle φ is varied in a Renninger experiment, successive three-beam interaction points of the reciprocal lattice are brought close to the Ewald sphere. In first-order theory, these effects are completely additive. Hence, at any general angle φ, the effective structure factor becomes a generalization of (16*b*), for example for the σ mode, of the form

$$F^{\sigma}_{HLM\ldots}=F_H-\frac{F_{\bar{L}}F_{L-H}}{2\tilde{\xi}_L}\Pi_1^L-\frac{F_{\bar{M}}F_{M-H}}{2\tilde{\xi}_M}\Pi_1^M-\ldots, \qquad (28)$$

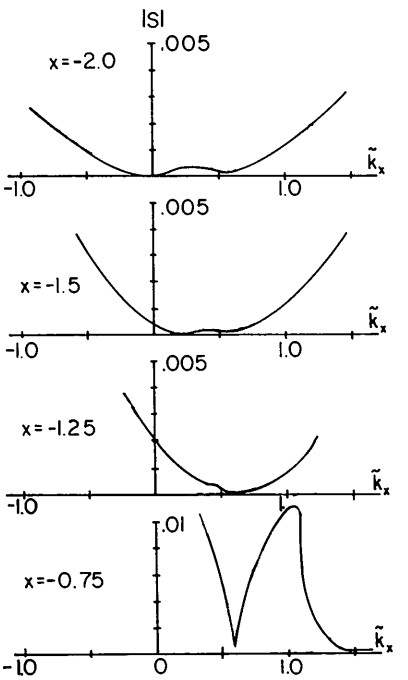

Fig. 3. Residual values $|S|$ of the right side of (18), a measure of the goodness of the first-order solution, for several x near $x=-1$, for the hypothetical strong reflection Ge 222/11$\bar{1}$ without absorption.

and similarly for the π mode. Other effects, such as the shift of the Lorentz point, are also additive. The integrated intensity in the $\mathbf{K}_H$ direction resulting from (28) follows by using (6). The angle φ_T in each of the $\tilde{\xi}_L$'s appearing in (9) is measured relative to its own three-beam angle φ_{TL}, and the Π_i's are determined by (15) separately for each interacting triplet. Generally, only one of the $\tilde{\xi}_L$'s will be small in the neighborhood of any one three-beam point, so that its contribution predominates. All other neighboring three-beam points give corrections, which, because the entire diffraction process is coherent, are added in (28) rather than as separate intensities.

This procedure has been applied to calculate the pattern of five neighboring three-beam interactions of Ge 222, since high-resolution experimental data for this group have recently become available (Nicolosi, 1982). Fig. 4 is a copy of some of the data of Fig. 18 of that reference, and Fig. 5 shows the calculated pattern, assuming unpolarized incident radiation, based on the data for each of the three-beam points listed in Table 3. The only adjustment involves a translation from our φ scale of Fig. 1 to that used in the experiment, $\varphi_{\rm exp} = 30° - \varphi$. All other features, such as the relative asymmetries, the widths of the reflections, the long tails and the changes in level of the 'primary' reflection background between peaks, are completely determined by the input data of Table 3. The overall agreement is very satisfactory, considering that no experimental divergences have been included in Fig. 5. These probably mask the dips for the $1\bar{3}3$ and $3\bar{1}\bar{3}$ points. The absence in Fig. 4 of the pronounced minimum predicted for the $7\bar{1}1$ point, though, may indicate the importance of higher-order influences in certain reflections. In Fig. 5, all θ_L's are small enough so that for each peak the σ and π dips lie on the same side, but, since they occur at different φ, some of the sharp features predicted for polarized radiation average out. [For high θ_L, where the two dips can be on opposite sides, some minima may then become obscured altogether. Clearly, unpolarized incident radiation may cause a substantial loss of information whenever the π mode can mask the asymmetry of the σ mode. This is especially serious in noncentrosymmetric crystals, where all asymmetries are expected to be less pronounced (Juretschke, 1982*b*).]

Table 3. *Numerical inputs for a sequence of* Ge 222/*L interactions*

$L=$	$3\bar{1}\bar{3}$	$11\bar{1}$	$1\bar{3}3$	$7\bar{1}1$	$3\bar{5}1$
F'_L	103	151	103	64	79
F'_{L-H}	79	−121	−90	79	64
$\varphi_{TL}(°)$	7·77	5·43	3·47	2·16	−2·16
$30°-\varphi_{TL}(°)$	22·23	24·57	26·53	27·84	32·16
$\varphi_L(°)$	−90·13	−27·80	79·90	−150·30	150·30
$\theta_L(°)$	−38·98	−18·33	−18·33	38·98	−38·98
Π_1	0·3956	0·8040	0·1266	0·8516	0·8516
Π_6	0·2472	0·6350	0·4841	0·3487	0·3487
$(\tan\varphi/x)_L$	$-2·76\times10^{-4}$	$2·21\times10^{-3}$	$-8·37\times10^{-5}$	$-7·45\times10^{-4}$	$7·45\times10^{-4}$

Equation (28) also contains the long tails seen experimentally, and found by computer simulation (Chapman, Yoder & Colella, 1981), as a natural consequence of conventional dynamical theory that conserves both energy and momentum. These tails can produce pronounced steps, even between peaks several degrees apart. Their range will be the larger, the smaller the F_H of the primary reflection, and may have to be taken into account when determining very small structure factors (Mills & Batterman, 1980).

B. Four- or higher-beam cases

In first-order theory, four-beam cases are described by the coalescence of two three-beam points, such that, for example, in (28), $\varphi_{TL} = \varphi_{TM}$. Now, two of the $\tilde{\xi}_L$'s in (28) will be large in the neighborhood of the common three-beam point. The effective structure factor is then determined by the weighted contribution of these two three-beam couplings, depending on their F triplets, and on their respective geometrical

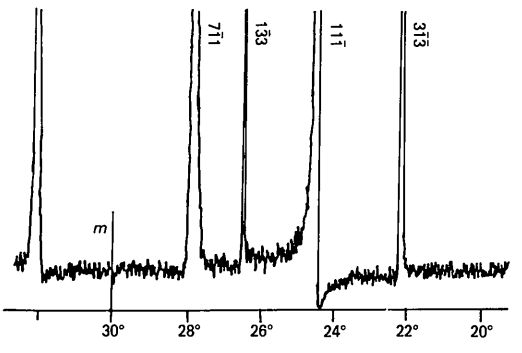

Fig. 4. Experimental Renninger chart for Ge 222/*L* reproduced from Fig. 18 of Nicolosi (1982).

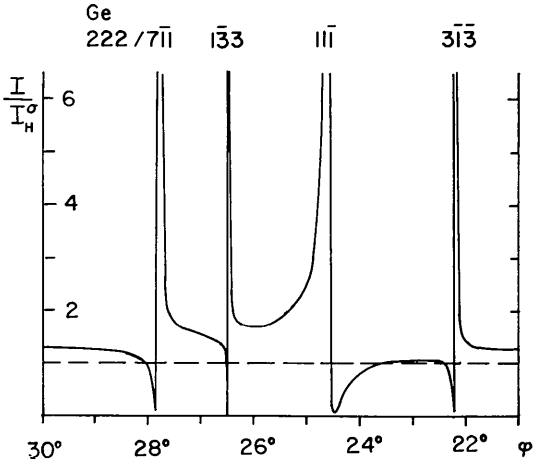

Fig. 5. Theoretically predicted Renninger chart for four peaks of Fig. 4, using (28) and (6) with the inputs of Table 3, for unpolarized incident radiation. The two-beam primary reflection I_H^σ is taken as unity.

factors. This approach to analyzing four-beam interactions has been found to work well experimentally (Gong, 1983), when the two contributions have the same sign.

The extension of this argument to $n > 4$ is obvious.

C. $F_H = 0$

If the primary reflection vanishes, the first-order solution of § 5 in terms of the quasi-universal scale x no longer applies, because the transformation to this scale becomes singular. However, all equations of § 4 are still valid, with the new feature that, for example in (17), all fields are now multiplied by factors of similar magnitude. First-order perturbation breaks down, and the coupling between the σ and π modes cannot be neglected at any stage of approximation. We are always in the regime $x \ll 1$ of the simple formulation that forms the basis of this paper.

9. The physics of the first-order solution

The two central features of the first-order solution discussed here are, first, that there exists a quasi-universal scale, the x scale of (22), for measuring the strength of the coupling and, second, that for $|x| \geq 1$ the main effect of this coupling is a modified structure factor, (16*b*), in an otherwise normal two-beam case.

The universal scaling depends on the relative scattering strength $F_L F_{\bar{L}-\bar{H}}/F_H$, and also normalizes the motion of **L** across the Ewald sphere relative to changes in φ. Its other angular factors are related to polarization effects.

The modification of the structure factor implies that initially the coupling distorts the two-beam dispersion surface in a manner preserving the two-beam character and, depending on the gap width, either more or less energy is sent into the $\mathbf{K}_H$ direction.

To illustrate these distortions, we have computed the real part of the σ and π dispersion surfaces for several x, for the hypothetical case of Ge 222/11$\bar{1}$ with negligible absorption. Fig. 6 shows the results for the symmetric Bragg case in a semi-infinite crystal. It demonstrates both the shift of the Lorentz points, different for σ and π, and the width of the totally reflecting regions, as they vary with x. The curves exemplify the initial stage of the topological distortions already discussed by Fues (1938), and later by Stern, Perry & Boudreaux (1969).

Following Kambe & Miyake (1954), the effects of this distortion can also be described by plotting the opposite edges of the totally reflecting regions of Fig. 6 as a function of x. This is shown in Fig. 7. The asymmetry of the width of the reflecting region (and therefore of the integrated intensity) is clearly brought out, and the vanishing of both reflections occurs close to $x = -1$, where the edges cross. This crossing is reminiscent of the crossing of bands in the electron theory of metals and, in fact, represents a similar phenomenon: under certain conditions the structure factor for a particular reflection vanishes, and with it the gap in the band structure. Bloch waves consisting of single plane waves can propagate, and no diffraction occurs.

From this point of view, interference is not the primary cause (Hümmer & Billy, 1982) of the asymmetry of the integrated reflected intensity, but results from the effects of the distortion on the modes of propagation. In addition, modifications of the dispersion surface, such as in Figs. 6 and 7, are largely independent of absorption, so that absorption is not fundamental in explaining the asymmetric features of the reflected intensity in the angular range near $x = -1$, certainly in perfect crystals.

Figs. 6 and 7, and their implications, are exact only for the first-order solution, as they would be for strict two-beam cases. Many of their extreme features will be softened by including absorption. Beyond that, the coupling of the σ and π modes in the full solution will remove the degeneracies at the crossing of the band edges, so that there will probably always remain

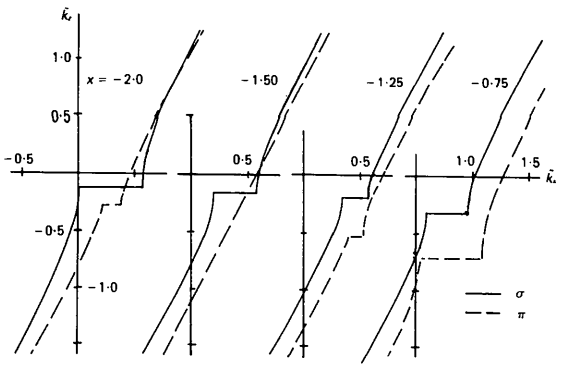

Fig. 6. Real part of the σ and π dispersion surfaces exciting fields in a semi-infinite crystal, for the first-order solution of the hypothetical Ge 222/11$\bar{1}$ strong interaction. The horizontal portions are the regions of total reflection.

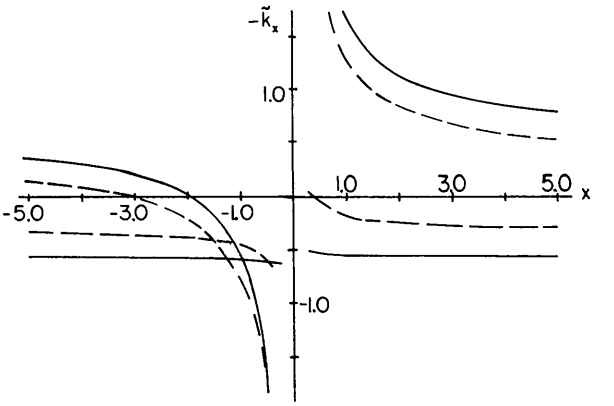

Fig. 7. Edges of the totally reflecting regions of Fig. 6 *vs* x. These curves also represent the intersections of the two-beam planes of incidence with the dispersion surface obtained when the geometrical three-beam point is at the origin, and projected on $\tilde{k}_z = 0$. The direction $-\tilde{k}_x$ points towards the Laue line.

finite but small gaps. Since the coupling between first-order modes becomes important near the crossing, the normal modes in this region have elliptical polarization varying with the angle of incidence, and a more careful analysis is needed to obtain accurate fields and intensities. In particular, the polarization composition of reflected intensities from unpolarized sources becomes very complex around $x = -1$, and simple conceptual interpretations of three-beam effects using plane polarized modes and based on unpolarized incident radiation become inadequate.

As the details of the various crossings, such as in Fig. 6, depend intricately on the parameters of every specific three-beam case, it is unlikely that next-order perturbation solutions can be cast in the same universal form as the solutions discussed here.

In any case, since higher-order effects become important only in the region $|x| \lesssim 1$, they in no way obscure the major asymmetries at the heart of the first-order solutions that should be observable under good experimental conditions at much larger x.

This work was partly supported by Joint Services Electronics Program Contract No. F49620-82-C-0084. We also thank the referee for calling our attention to the paper by Watanabe *et al.*

References

AFANAS'EV, A. M. & PERSTNEV, I. P. (1969). *Acta Cryst.* A**25**, 520–523.

BATTERMAN, B. W. & COLE, H. (1964). *Rev. Mod. Phys.* **36**, 681–717.

BETHE, H. A. (1928). *Ann. Phys. (Leipzig)*, **87**, 55–129.

BONSE, U. & HART, M. (1965). *Appl. Phys. Lett.* **6**, 155–156.

BORRMANN, G. (1950). *Z. Phys.* **42**, 157–162.

CHANG, S. L. (1982). *Phys. Rev. Lett.* **48**, 163–166.

CHAPMAN, L. D., YODER, D. R. & COLELLA, R. (1981). *Phys. Rev. Lett.* **46**, 1578–1581.

COLELLA, R. (1974). *Acta Cryst.* A**30**, 413–423.

COWAN, P. L., GOLOVCHENKO, J. A. & ROBBINS, M. F. (1980). *Phys. Rev. Lett.* **44**, 1680–1683.

EWALD, P. P. (1916). *Ann. Phys. (Leipzig)*, **49**, 1–38.

EWALD, P. P. & HÉNO, Y. (1968). *Acta Cryst.* A**24**, 5–15.

FUES, E. (1938). *Z. Phys.* **109**, 236–259.

GJØNNES, J. (1962). *Acta Cryst.* **15**, 703–707.

GONG, P. P. (1983). PhD Thesis, Polytechnic Institute of New York.

HILDEBRANDT, G. (1967). *Phys. Status Solidi*, **24**, 245–261.

HILDEBRANDT, G. (1982). *J. Phys. E*, **15**, 1140–1155.

HÜMMER, K. & BILLY, H. W. (1982). *Acta Cryst.* A**38**, 841–848.

JAMES, R. W. (1963). *Solid State Phys.* **15**, 53–220.

JURETSCHKE, H. J. (1982*a*). *Phys. Rev. Lett.* **48**, 1487–1489.

JURETSCHKE, H. J. (1982*b*). *Phys. Lett.* **92A**, 183–185.

JURETSCHKE, H. J. & WASSERSTEIN-ROBBINS, F. (1982). *Phys. Rev. B*, **26**, 4262–4268.

KAMBE, K. & MIYAKE, S. (1954). *Acta Cryst.* **7**, 218–219.

KOHN, V. G. (1979). *Phys. Status Solidi A*, **54**, 375–384.

LAUE, M. VON (1960). *Roentgenstrahl-Interferenzen.* Frankfurt (Main): Akademische Verlagsgesellschaft.

LEROUX, S. D., COLELLA, R. & BRAY, R. (1975). *Phys. Rev. Lett.* **35**, 230–234.

MILLS, D. & BATTERMAN, B. W. (1980). *Phys. Rev. B*, **22**, 2887–2897.

NICOLOSI, J. (1982). PhD Thesis, Polytechnic Institute of New York.

POST, B. (1979). *Acta Cryst.* A**35**, 17–22.

STERN, R. M., PERRY, J. J. & BOUDREAUX, D. S. (1969). *Rev. Mod. Phys.* **41**, 275–295.

UEBACH, W. (1973). *Z. Naturforschung. Teil A*, **28**, 1214–1220.

WATANABE, D., UYEDA, R. & KOGISO, M. (1968). *Acta Cryst.* A**24**, 249–250.

Acta Cryst. (1984). A**40**, 389–394

The Distribution of $\alpha_{\mathbf{h}}$

BY G. CASCARANO AND C. GIACOVAZZO

Dipartimento Geomineralogico, Università, 70121 *Bari, Italy*

M. C. BURLA AND A. NUNZI

Istituto di Mineralogia dell'Università, 06100 *Perugia, Italy*

AND G. POLIDORI

Centro di Calcolo Elettronico dell'Università, 06100 *Perugia, Italy*

(*Received* 13 *October* 1983; *accepted* 25 *January* 1984)

Abstract

The asymptotic distribution of $\alpha_{\mathbf{h}}$ is calculated *via* the distribution of the resultant of complex random vectors whose phase values are distributed according to Von Mises distributions. The statistical results suggest that the phase of the resultant, say $\theta_{\mathbf{h}}$, is distributed around the phase $\varphi_{\mathbf{h}}$, approximately according to a Von Mises distribution.

Introduction

When several pairs of phases $\varphi_{\mathbf{k}_j}$, $\varphi_{\mathbf{h}-\mathbf{k}_j}$ are known, the conditional probability distribution of the phase

0108-7673/84/040389-06$01.50